

Atomic Resolution Imaging of CrBr₃ using Adhesion-Enhanced Grids

*Matthew J. Hamer^{1,2}, David G. Hopkinson^{2,3}, Nick Clark^{2,3}, Mingwei Zhou^{1,2}, Wendong Wang^{1,2}
Yichao Zou³, Daniel J. Kelly^{2,3}, Thomas H. Bointon², Sarah J. Haigh^{2,3,**}, Roman V.
Gorbachev^{1,2,4,*}*

¹Department of Physics and Astronomy, University of Manchester, Oxford Road, Manchester,
M13 9PL, UK

²National Graphene Institute, University of Manchester, Oxford Road, Manchester, M13 9PL,
UK

³Department of Materials, University of Manchester, Oxford Road, Manchester, M13 9PL, UK

⁴Henry Royce Institute, Oxford Road, Manchester, M13 9PL, UK

*Roman@Manchester.ac.uk, **Sarah.Haigh@Manchester.ac.uk

**KEYWORDS: Magnetic 2D Materials, TEM, Graphene Encapsulation, Crystal Transfer,
Suspended Devices**

Abstract

Suspended specimens of 2D crystals and their heterostructures are required for a range of studies including transmission electron microscopy (TEM), optical transmission experiments and nanomechanical testing. However, investigating the properties of laterally small 2D crystal specimens, including twisted bilayers and air sensitive materials, has been held back by the difficulty of fabricating the necessary clean suspended samples. Here we present a scalable solution which allows clean free-standing specimens to be realized with 100% yield by dry-stamping atomically thin 2D stacks onto a specially developed adhesion-enhanced support grid. Using this new capability, we demonstrate atomic resolution imaging of defect structures in atomically thin CrBr₃, a novel magnetic material which degrades in ambient conditions.

Introduction

The family of 2D materials now includes over a hundred members, many of which have been isolated in monolayer form by mechanical exfoliation^{1,2}, direct chemical growth^{3,4} or solution-phase processing⁵. They possess a diverse range of electronic and optical properties, which can vary even for a single material depending upon thickness^{6,7} and stacking order^{8,9}. Most recently, 2D crystals with magnetic order have been identified, opening a wide range of possibilities for both fundamental research and applications¹⁰. To date, several of these magnetic van der Waals' materials have been isolated and characterized, including CrBr₃¹¹, CrI₃¹², CrGeTe₃¹³, MnPS₃¹⁴ and FePS₃¹⁵. These atomically thin crystals can exhibit both ferromagnetic and antiferromagnetic behavior with strong layer-dependence¹⁶ making them ideal as magnetic components within 2D heterostructure-based devices. For example, magnon-assisted electron scattering has been

observed in CrBr₃ tunnel barriers with graphene electrical contacts, allowing scope for spin injection into graphene¹⁷. One of the chief reasons for the relatively late emergence of these materials is their rapid structural and property degradation in ambient conditions, with all of the aforementioned crystals being sensitive to air, light and/or moisture. For example, CrI₃ is found to degrade quickly in ambient environments via photocatalytic substitution of iodine by water¹⁸. This necessitates a complex sample preparation route where samples are exfoliated in an inert gas environment and encapsulated with impermeable 2D materials in order to mitigate degradation^{18,19}. Unfortunately, such processing generates additional sample preparation challenges that have hindered characterization, including the use of transmission electron microscopy (TEM). Such TEM investigations would be highly desirable in order to study local defect structures including atomic edge reconstruction, grain boundaries, local ordering, adatom doping, and vacancy dynamics. The key hurdle for TEM experiments is producing large, flat and contamination-free suspended few-layer crystals without exposure to high temperatures or multiple cleaning steps which are liable to damage the material or break the encapsulation barrier²⁰. This problem is common to other characterization routes that require suspended 2D crystals, including nanomechanical testing²¹⁻²³ and transmission optical measurements²⁴. Here we outline a route to reliably fabricate clean free-standing specimens for air-sensitive 2D crystals with nearly 100% yield. This is achieved using a new adhesion-enhanced support grid (AEG), which consists of a Si/SiN_x substrate with added Cr, Au, and MoS₂ layers and which has the potential to be produced on a large-scale production *via* wafer scale processing. The ultra-flat MoS₂ surface provides improved van der Waals interaction such that the grids are compatible with the widely acclaimed dry-stamp transfer method¹⁹ for 2D heterostructure flake transfer. We demonstrate this new

approach by providing the first atomic resolution TEM studies of degradation, defects and stacking in the recently isolated, highly air-sensitive, magnetic 2D crystal, CrBr₃.

Main Body

Plan view TEM imaging of atomically thin crystals is achieved by suspending a specimen on a perforated support membrane. These support grids can comprise of Si/SiN_x, Si/SiO₂ or of a (holey) amorphous carbon membrane suspended over a metal mesh^{25,26}. The choice of grid and method used to obtain a free standing 2D crystal depends upon the experimental goals, the specimen and the local skill set. TEM specimens of liquid phase exfoliated crystals can be simply drop cast onto conventional support grids, and here the challenge is hunting for suitable areas of free-standing crystal and removing undesirable solvents that may hinder TEM investigations²⁷. However, for many exfoliated and grown 2D crystals, as well as all fabricated 2D heterostructures, the specimen is usually prepared using the wet transfer approach, which involves using a micromanipulation system to transfer a 2D crystal, attached to a polymer support layer, directly onto the TEM grid²⁸. To achieve high resolution imaging the polymer layer must be dissolved, leaving just the specimen suspended over the holes of the support grid²⁸. This technique has a number of problems: (1) poor adhesion between 2D crystals and the support grid often results in failed transfers as specimens delaminate or scroll (see **Supporting Information S2**), (2) solvent surface tension during the drying process often results in the rupturing of suspended regions^{29,30} and (3) incomplete removal of the polymer support layer frequently results in a 1-10 nm thick layer of surface contamination which prevents ultimate resolution TEM imaging^{31,32}. Contamination can often be removed with high temperature heat treatments or subsequent washing steps; but these are not suitable for all specimens, provide additional points of failure and can degrade the specimen composition. Taken

together these factors seriously limit the yield for successfully fabricating free-standing 2D crystals, wasting many thousands of research hours depending upon the type and size of the specimen (see **Table 1**). A more reliable method for specimen preparation is thus required to facilitate efficient TEM studies of many new 2D materials and their heterostructures, as well as for a broad range of optical and nanomechanical techniques where clean free-standing 2D crystals are employed.

Dry-stamp transfer has emerged as a clean, reliable and efficient method for manipulation of mechanically exfoliated 2D flakes³³, but this approach is not possible using conventional TEM supports. Here we present a novel support grid that is compatible with direct dry-stamp transfer, facilitating preparation of ultra-clean large area TEM specimens for air-sensitive 2D materials and complex heterostructures (**Figure 1**). We begin with a standard Si/SiN_x grid, which we chose to fabricate in-house to allow flexibility over the commercially available models. The Si/SiN_x grid was prepared by patterning a SiN_x/Si/SiN_x wafer using optical lithography and reactive ion etching (RIE) with a mixture of CHF₃ and O₂ to remove the exposed SiN_x. Following this, the sample was immersed in potassium hydroxide (KOH) to etch away the exposed bulk silicon leaving an isotropic etch profile as shown in **Figure 1a**. The sample was then flipped and the opposite SiN_x membrane patterned with an array of holes using optical lithography and the same RIE process (**Figure 1b**). The size of these holes was typically 1-5 μm diameter, providing a compromise between imaging area and specimen contact area (**Figure 1d**).

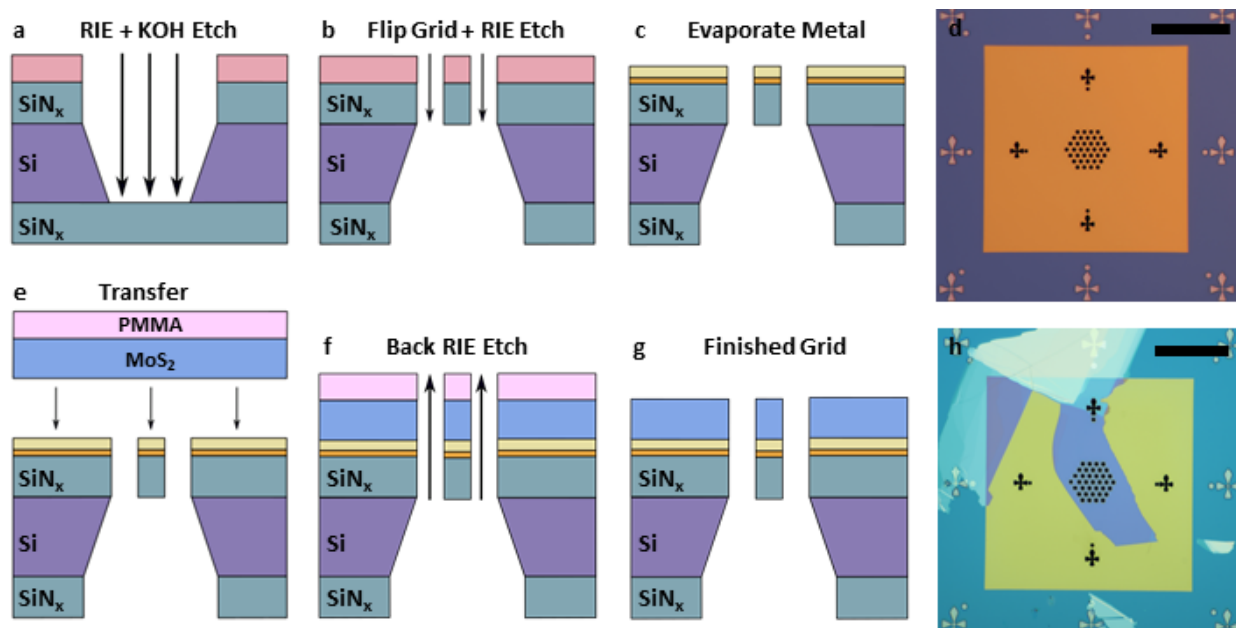


Figure 1. Fabrication procedure to create adhesion-enhanced MoS₂ grids. (a) First a SiN_x/Si/SiN_x wafer is coated with photoresist (pink layer) then patterned using photolithography. Then the SiN_x layer (teal) is removed by RIE and the exposed Si etched with KOH. (b) The grid is then flipped and the opposite side coated with photoresist. A grid pattern is written using optical lithography and RIE is then used to etch through the SiN_x. (c) Next Cr (1nm) and Au (5nm) adhesion layers are evaporated onto the grid with electron-beam evaporation. (d) Optical image of a patterned TEM grid. (e) In the next step a bulk crystal of mechanically exfoliated MoS₂ is transferred onto a grid using the PMMA dry-stamp transfer process. (f) The MoS₂ is back-etched through the grid. (g) The PMMA is dissolved in solvent and the grid is annealed at 450°C in 10% H₂/Ar to remove surface residue. (h) Optical image of a finished adhesion-enhanced grid. Scale bar in (d) and (h) is 20μm.

To enhance this conventional SiN_x grid design, a thin layer of chromium (1 nm) followed by gold (5 nm) was deposited onto the surface using electron-beam evaporation (**Figure 1c**). A large bulk MoS₂ crystal (>10 nm thickness, >50 μm x 50 μm in lateral area) was then transferred onto the

grid using the poly(methyl-methacrylate) (PMMA) dry-stamp transfer technique¹⁹ and a micromanipulation setup³⁴ (**Figure 1e**). The suspended regions of MoS₂ over the holes in the SiN_x were then etched away using RIE from the back side of the grid with the SiN_x serving as an etch mask (**Figure 1f**). Finally, the PMMA transfer layer was dissolved and the grid annealed at 450°C in 10% H₂/Ar for 6 hours (**Figure 1g**) to remove chemical residues and help bond the MoS₂ crystal to the SiN_x by partial melting of the gold layer. We have found that annealing temperatures of at least 400°C are required to effectively bond the MoS₂, consistent with the expected melting point of thin Au films³⁵. An optical image of the complete adhesion-enhanced grid (AEG) support is shown in **Figure 1h**. An extended description of the method is provided in **Supporting Information S1**.

A key advantage of our AEGs is their much lower surface roughness compared to SiN_x grids or traditional holey carbon grids, achieved by the presence of the atomically smooth MoS₂. The roughness is greatly reduced at both the nanometer and micrometer length scales (**Figure 2**), which increases the van der Waals interaction between the grid and the 2D material or heterostructure specimen. Atomic force microscope (AFM) characterization of multiple areas on multiple grids gives an RMS roughness for our AEG grid of approximately 45 pm (the resolution limit of the AFM) compared to 320-450 pm for the SiN_x, and >800 pm for the carbon films tested. This improves the adhesion of atomically thin samples to the grids, reducing the probability of delamination or scrolling during removal of the polymer support film. Intrinsically better adhesion also removes the need for high temperature annealing as part of the transfer which, although it can improve specimen adhesion, is potentially damaging for heat sensitive samples. Importantly, the improved adhesion means our AEG supports are compatible with the dry-stamp mechanical

transfer³³, which leaves significantly less polymer residue compared to conventional transfer¹⁹. This process relies on van der Waals attraction between the specimen and the substrate being stronger than between the specimen and the polymer support film, so that the specimen preferentially adheres to the substrate (see **Supporting Information S3**). We have found dry-transfer is not compatible with conventional TEM support grids: due to the small effective contact area the specimen remains attached to the polymer rather than the grid, or the polymer only partially delaminates causing damage to both the crystal and the grid.

We also tested the potential of other environmentally and thermally stable 2D materials for the 2D adhesion layer as alternatives to MoS₂. Hexagonal boron nitride (hBN) yielded similar positive transfer results, yet its insulating behavior made it unattractive for TEM studies where a conducting support helps to prevent specimen charging artefacts. Using graphite resulted in unwanted ‘fencing’ along the edges of the holes, providing additional roughness which interfered with subsequent transfers of the 2D crystal or heterostructure specimens (see **Supporting Information S4**). An additional benefit of using MoS₂ is its scalability, as few-layer uniform films produced by chemical vapor deposition (CVD) are becoming commercially available³⁶.

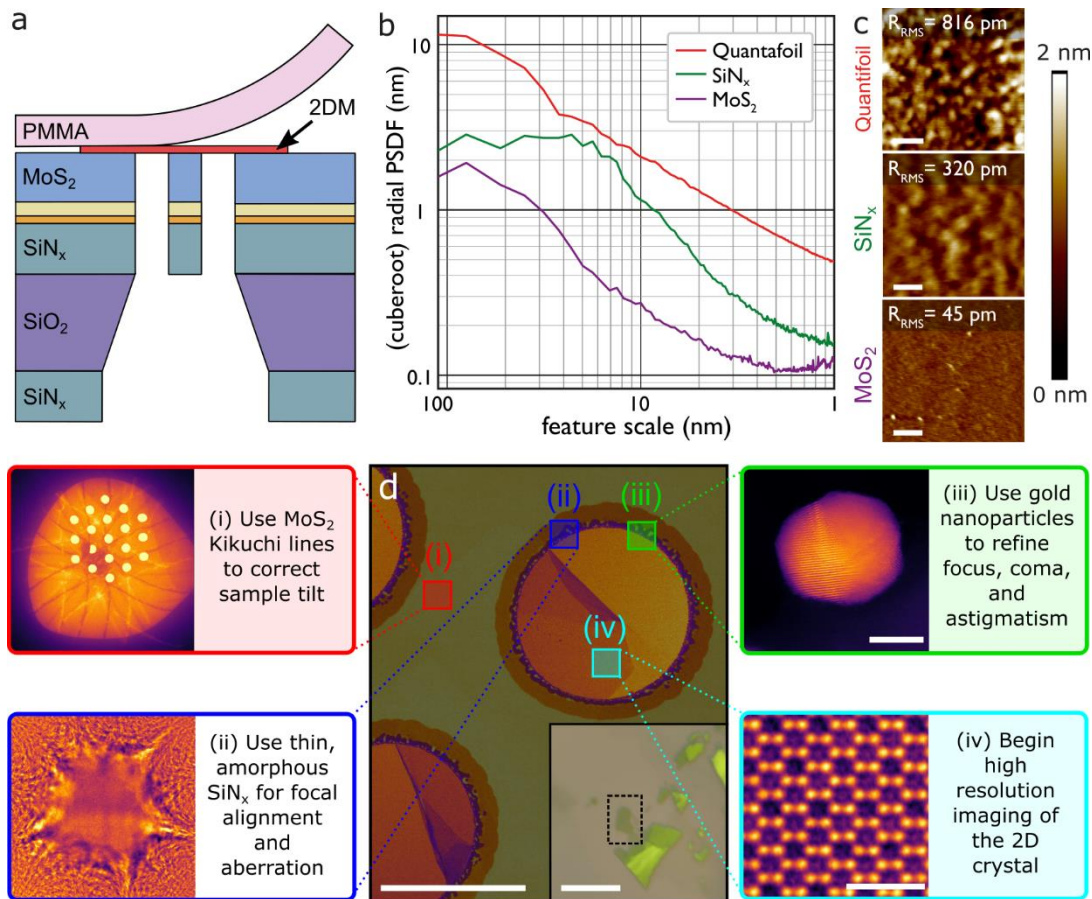


Figure 2. Sample transfer onto an AEG support. (a) Schematic of a 2D material dry-stamp transfer onto an AEG. The red layer is the transferred 2D specimen (2DM), the pink layer is the transfer polymer. (b) AFM roughness analysis comparing MoS₂, SiN_x and Quantifoil TEM grids over different length scales and (c) surface roughness comparison taken over representative 500x500nm sampling areas. (d) False color STEM image of a 2D sample on an AEG, inset optical image of sample prior to AEG transfer (sample indicated by black dashed rectangle): (i-iv) a hierarchical approach to STEM imaging alignment using the structural features of an AEG. Scale bars (c) 100 nm, (d) 2 μ m, (d inset) 5 μ m, (iii) 5nm and (iv) 1nm.

In addition to the aforementioned benefits for sample fabrication, AEGs provide multiple practical advantages for effective high resolution TEM and scanning transmission electron microscopy

(STEM). Our developed hierarchical route to optimal STEM imaging is presented in **Figure 2d** where different components of the AEG are used to optimize the microscope set-up without compromising potential areas of interest. In brief the process is: **(i)** correct global sample tilt onto the desired [001] zone axis using the Kikuchi bands from the MoS₂ in the Ronchigram, **(ii)** set sample height and correct probe aberrations using thin, amorphous SiN_x at the edge of the holes, **(iii)** fine-tune axial coma and astigmatism in the probe using Au nanoparticles in imaging mode, **(iv)** move to specimen area with optimized imaging conditions. Even in the latest generation of aberration corrected electron microscopes aberrations tend to drift from their optimal values, so optimal imaging conditions are only stable for minutes to hours³⁷. The ability to correct for unwanted low order aberrations (e.g. defocus, astigmatism and axial coma) using the edge of the ultra-thin SiN_x support and the Au nanoparticles, close to the region of interest is thus highly desirable, especially for the most electron beam sensitive 2D crystal samples. Furthermore, the very flat grid provides minimal variations in specimen tilt and height over distances of several microns, reducing the need to regularly reorient the sample and facilitating automated imaging procedures. The false-color STEM image is constructed using the method described in **Supporting Information S5**.

We have tested the efficacy of our AEGs on a wide range of 2D materials and heterostructure samples. We find that the overall success rate of specimen transfer is 97%, (2 failures from 67 sample transfers), compared to just 36% when transferring to uncoated SiN_x TEM grids (39 failure from 58 samples, see **Table 1** for details). For both conventional grids and AEGs these results are based upon data collected from 10 individuals with experience of over 100 2D crystal transfers. Furthermore, the original uncoated SiN_x grid transfer approach was already optimized based on

many years' experience³⁸. For example, we find that graphene encapsulation of air sensitive crystals increases the effective sample area, which increases the success rate of specimen transfer, in addition to the other previously reported benefits of charge dissipation³⁹ and use as a protective barrier²⁰. However, the additional transfer steps associated with graphene encapsulation may also introduce additional contamination so is not always desirable. It is therefore most encouraging that the greatest improvement in transfer success rates is seen for laterally small 2D crystals or heterostructure stacks. Specimens with lateral sizes of $\sim 5\mu\text{m}$ or below, such as twisted MoS_2/WS_2 bilayers⁴⁰, are indicated in **Table 1** and for these samples the success rate improves from 15% to 94% using the AEG approach.

Table 1. Transfer statistics comparing samples transferred onto SiN_x grids and AEG supports. * indicates specimens with smaller areas due to the absence of graphene (Gr).

Material	Attempts with SiN_x Grid	Success rate with SiN_x Grids (%)	Attempts with MoS_2 Grids	Success rate with MoS_2 Grids (%)
Gr	10	60	10	100
Gr/ CrBr_3 /Gr	4	50	5	100
Gr/ CrGeTe_3 /Gr	4	50	5	100
Gr/ InSe /Gr ²⁰	8	50	6	100
Gr/ GaSe /Gr ²⁰	6	50	6	100
ZIF-7*	6	50	5	100
Mica*	10	10	10	90
MoS_2/WS_2 * ⁴⁰	10	0	20	95
All grids	58	36	67	97

We illustrate the benefit of our AEGs by using them to enable STEM imaging of the air-sensitive magnetic 2D crystal CrBr_3 (see **Figure 3**). The few-layer specimen was prepared by micromechanical exfoliation in an inert argon glovebox³⁴, followed by graphene encapsulation, removal from the glovebox and dry-transfer on to a AEG. We have found that few-layer CrBr_3

crystals are sensitive to even moderately elevated temperatures thus annealing was avoided during the whole fabrication process. An extended description of the TEM/STEM methods is provided in **Supporting Information S6**.

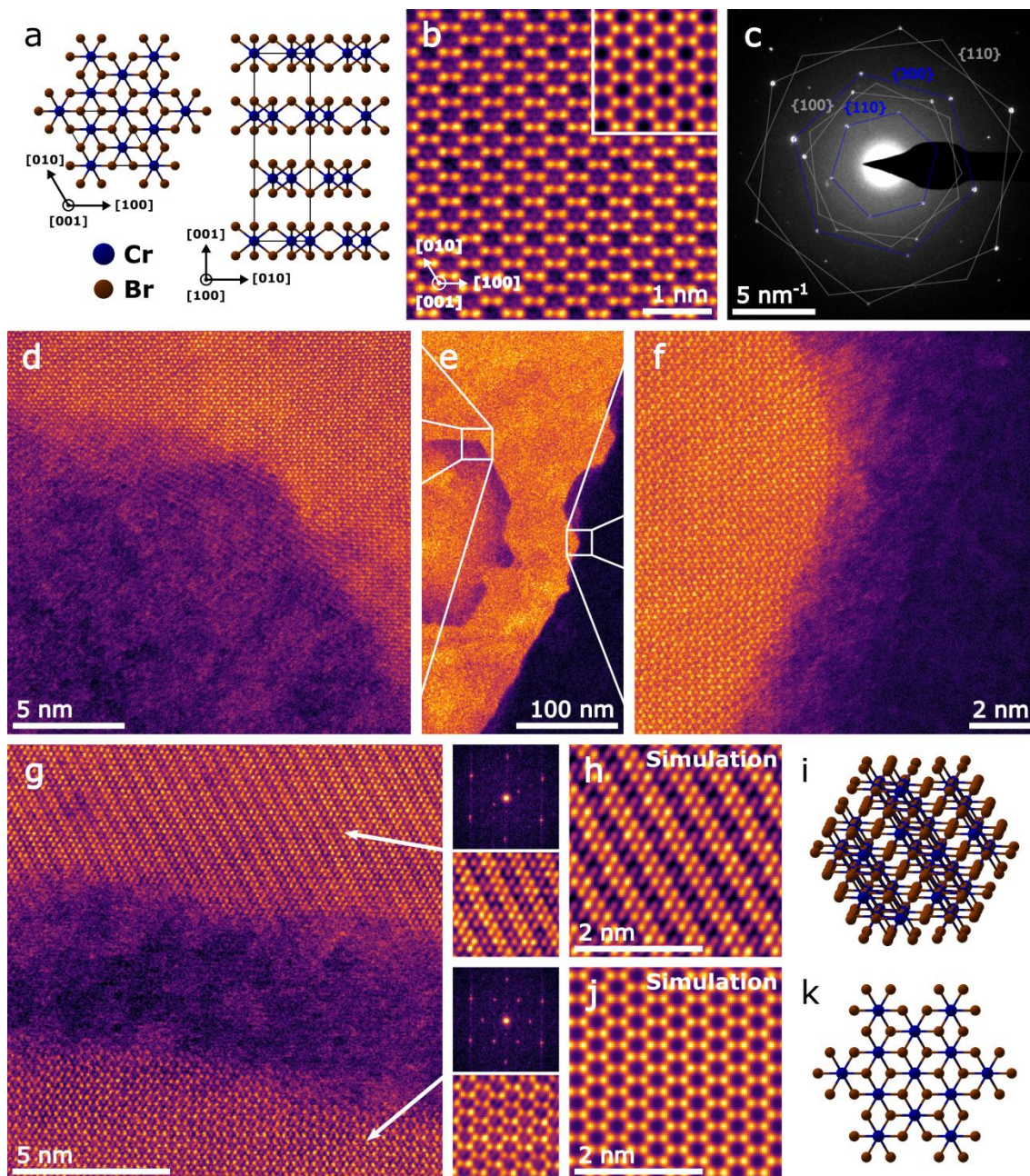


Figure 3. Atomic resolution ADF-STEM imaging of few-layer CrBr₃ crystals. (a) Model of trigonal CrBr₃, with unit cell dimensions indicated with black lines. (b) Drift-corrected, time-averaged, atomic resolution ADF-STEM image of 4-layer CrBr₃, showing strong agreement with image simulation (inset). (c) SAED pattern of a few-layer crystal with 1st and 2nd order spots for CrBr₃ (blue) and the graphene encapsulation (grey) indicated. (d – f) Faceted degradation observed in few-layer CrBr₃, with details (d, f) of the regions highlighted in (e). (g) 6-layer thick trigonal (lower) and monoclinic (upper) stacked regions of crystal separated by a crack, with Butterworth-filtered reduced FFTs (field-of-view: 14.5 nm⁻¹) and details (field-of-view: 2 nm) highlighting the difference in symmetry. (h-k) ADF-STEM image simulation and atomic model of 6-layer monoclinic (h,i) and trigonal (j,k) CrBr₃. The monoclinic stacking is observed at a small tilt ($\sim 2.5^\circ$) towards the [890] direction.

The specimens contained large, atomically clean areas suitable for high resolution (S)TEM imaging (**Figure 3**), which has not been reported previously for this class of material. Selected area electron diffraction (SAED) (**Figure 3c**) revealed successful preservation of the crystal structure at the micrometer scale *via* graphene encapsulation,^{28,39}. The local thickness of the crystal was found to vary between 4 and 6 atomic layers, confirmed by comparison with atomic resolution image simulations as well as optical image contrast prior to encapsulation. The atomic number sensitivity of ADF-STEM imaging means that the two graphene encapsulation layers are virtually invisible and has negligible effect on image simulations where the elemental species of interest are significantly higher in atomic number than carbon²⁰. Preventing structural degradation of CrBr₃ is a key concern for the application of this material so it is informative to consider what can be learned about this from STEM characterization of encapsulated samples. Even when graphene encapsulation is performed in an inert atmosphere, oxygen containing surface species are often

trapped beneath the encapsulation layers and these tend to aggregate at edges of the specimen, in cracks or as pockets⁴¹ on the surface. For air sensitive materials like CrBr₃ interaction with trapped oxidizing species causes local degradation as shown in **Figure 3e**. Interestingly, unlike in similar graphene encapsulated crystals of black phosphorus⁴² and TaS₂⁴³, we observe that in CrBr₃, the boundaries of the degraded regions are highly faceted, preferring to terminate along the armchair directions (the {100} and {010} planes of the crystal), seen both at holes formed in the center of the crystal (**Figure 3d**) and at edges (**Figure 3f**). As holes in the center of a crystal are attributed to electron beam induced reaction of CrBr₃ with oxidizing species in trapped contamination pockets, their faceting confirms the phenomena is degradation induced, rather than a property of the crystal growth or of the mechanical exfoliation process. Although, the edge terminations are clearly crystallographically defined at the nanoscale, atomic resolution imaging suggests that the faceting is not atomically sharp. To further investigate the edge structure, we have performed STEM elemental mapping using electron energy loss and energy dispersive x-ray spectroscopy (EELS/EDXS) (see **Supporting Information S7**). This revealed a decrease in Br concentration relative to pristine CrBr₃, with a Cr:Br ratio of 1:2.5 at the edge versus 1:3 in the center, suggesting that Br is preferentially lost from the crystal and leaving Br vacancies in the edge region. The loss of Br is not unexpected as this element is known to readily intercalate into graphite⁴⁴ and therefore can easily diffuse away between the encapsulating graphene sheets. Unexpectedly we detect no significant oxygen layer associated with the crystal edges, which is in strong contrast with what is observed for other graphene encapsulated air sensitive crystals^{42,43}. Instead we observe only a carbon rich layer at the edge of the crystal, which is likely to be associated with a small amount of residual polymer contamination. We speculate that this could play a role in stabilizing the Br

vacancies and faceted edges, although first principles calculations would be required to better understand this behavior.

Our atomic resolution ADF-STEM imaging reveals the expected trigonal crystal stacking in the majority of the sample (**Figure 3b**)⁴⁵⁻⁴⁷. However, in **Figure 3g**, the stacking is seen to transition from the trigonal sequence (lower region) to a monoclinic sequence (upper region), with the two separated by a crack in the crystal. The differences in crystal symmetry are highlighted in the inset reduced Fast Fourier Transforms (rFFTs), where the change in stacking affects the intensity of the inner spots. This change in stacking is confirmed by comparison with image simulations (**Figure 3h, j**), which reveals that the stripe contrast is caused by the alignment of mixed Cr – Br (higher total Z, bright stripes) and Br – hollow site (lower total Z, dark stripes) atomic columns in this stacking. This sequence is similar to previously reported monoclinic CrX₃ (X = Cl, Br, or I)^{48,49} (an atomic model is presented in **Supporting Information S8/S9**, where we also compare the change in stacking to the strip contrast that can be produced by crystal tilt alone). Although local stacking changes can result during synthesis of 2D materials, the transition from trigonal to monoclinic can be achieved solely through shear forces, and the proximity of this structure to the crack suggests that here the transition is likely to be due to mechanical deformation resulting in the local slippage of atomic layers on one side of the crack.

Conclusion

In summary, we present a new design of adhesion-enhanced support grids that facilitate the clean and reliable preparation of suspended samples for 2D crystals and their complex heterostructures by the dry-stamp transfer method. These AEGs supports can be produced in bulk using traditional clean room fabrication processes and production could be scaled up to wafer scale through the use

of CVD MoS₂. We find the specimen preparation approach facilitated by the use of such grids has a 100% success rate for graphene encapsulated samples and 94% success rate for 2D crystals and heterostructures with small lateral dimensions. This much improved reliability compared to conventional support grids is invaluable when preparing free-standing specimen from the most challenging air-sensitive 2D crystals and sophisticated heterostructures. We demonstrate the successful application of our technique by atomic resolution STEM imaging of few-layer CrBr₃ films, revealing a range of new local structural detail including faceted crystal degradation and mechanically induced stacking faults.

Supporting Information. **S1** describes the adhesion-enhanced grid fabrication methodology. **S2** discusses scrolling effects on low adhesion TEM grids. **S3** demonstrates stamp transfer onto adhesion-enhanced grids. **S4** compares alternative materials for TEM grids. **S5** provides low magnification STEM data. **S6** displays CrBr₃ EELS/EDX data. **S7** describes the TEM/STEM methodology. **S8** and **S9** provide additional details about the TEM investigations.

AUTHOR INFORMATION

Corresponding Author

Roman Gorbachev

Roman@Manchester.ac.uk

Sarah Haigh

Sarah.Haigh@Manchester.ac.uk

Author Contributions

R.G. and S.J.H conceived the study; M.Z fabricated devices with help from M.H, N.C, T.B and W.W. TEM investigations of the samples were performed by D.G.H, D.K and Y.Z. The manuscript was written by M.H, N.C, D.G.H, S.J.H and R.G with contributions from all authors.

Funding Sources

We acknowledge support from EPSRC grants EP/N509565/1, EP/P01139X/1, EP/N010345/1 and EP/L01548X/1 along with the CDT Graphene-NOWNANO, and the EPSRC Doctoral Prize Fellowship. We thank Diamond Light Source for access and support in use of the electron Physical Science Imaging Centre (Instrument E02 and proposal numbers EM19315 and MG21597) that contributed to the results presented here. In addition, we acknowledge support from the European Commission including H2020 program grants: European Graphene Flagship Project (696656), European Quantum Technology Flagship Project 2DSIPC (820378), ERC Synergy Grant Hetero2D and ERC Starter grant EvoluTEM (715502).

Notes

Additional data related to the paper may be requested from the authors. The authors declare no competing financial interests.

REFERENCES

- (1) Novoselov, K. S.; Mishchenko, A.; Carvalho, A.; Castro Neto, A. H. 2D Materials and van der Waals Heterostructures. *Science* **2016**, 353 (6298), aac9439.
- (2) Butler, S. Z.; Hollen, S. M.; Cao, L.; Cui, Y.; Gupta, J. A.; Gutie, H. R.; Heinz, T. F.;

- Hong, S. S.; Huang, J.; Ismach, A. F.; et al. Progress, Challenges, and Opportunities in Two-Dimensional Materials Beyond Graphene. *ACS Nano* **2013**, 7 (4), 2898–2926.
- (3) Cai, Z.; Liu, B.; Zou, X.; Cheng, H. M. Chemical Vapor Deposition Growth and Applications of Two-Dimensional Materials and their Heterostructures. *Chem. Rev.* **2018**, 118 (13), 6091–6133.
- (4) Chhowalla, M.; Shin, H. S.; Eda, G.; Li, L.-J.; Loh, K. P.; Zhang, H. The Chemistry of Two-Dimensional Layered Transition Metal Dichalcogenide Nanosheets. *Nat. Chem.* **2013**, 5 (4), 263–275.
- (5) Nicolosi, V.; Chhowalla, M.; Kanatzidis, M. G.; Strano, M. S.; Coleman, J. N. Liquid Exfoliation of Layered Materials. *Science* **2013**, 340 (6139), 1226419.
- (6) Mattheiss, L. F. Band Structures of Transition-Metal-Dichalcogenide Layer Compounds. *Phys. Rev. B* **1973**, 8 (8), 3719–3740.
- (7) Hamer, M. J.; Zultak, J.; Tyurnina, A. V.; Zólyomi, V.; Terry, D.; Barinov, A.; Garner, A.; Donoghue, J.; Rooney, A. P.; Kandyba, V.; et al. Indirect to Direct Gap Crossover in Two-Dimensional InSe Revealed by Angle-Resolved Photoemission Spectroscopy. *ACS Nano* **2019**, 13 (2), 2136–2142.
- (8) Kappera, R.; Voiry, D.; Yalcin, S. E.; Branch, B.; Gupta, G.; Mohite, A. D.; Chhowalla, M. Phase-Engineered Low-Resistance Contacts for Ultrathin MoS₂ Transistors. *Nat. Mater.* **2014**, 13 (12), 1128–1134.
- (9) Ayari, A.; Cobas, E.; Ogundadegbe, O.; Fuhrer, M. S. Realization and Electrical Characterization of Ultrathin Crystals of Layered Transition-Metal Dichalcogenides. *J. Appl. Phys.* **2007**, 101 (1), 014507.
- (10) Burch, K. S.; Mandrus, D.; Park, J. G. Magnetism in Two-Dimensional van der Waals

- Materials. *Nature* **2018**, *563* (7729), 47–52.
- (11) Kim, M.; Kumaravadivel, P.; Birkbeck, J.; Kuang, W.; Xu, S. G.; Hopkinson, D. G.; Knolle, J.; McClarty, P. A.; Berdyugin, A. I.; Ben Shalom, M.; et al. Micromagnetometry of Two-Dimensional Ferromagnets. *Nat. Electron.* **2019**, *2* (10), 457–463.
- (12) Huang, B.; Clark, G.; Klein, D. R.; MacNeill, D.; Navarro-Moratalla, E.; Seyler, K. L.; Wilson, N.; McGuire, M. A.; Cobden, D. H.; Xiao, D.; et al. Electrical Control of 2D Magnetism in Bilayer CrI₃. *Nat. Nanotechnol.* **2018**, *13* (7), 544–548.
- (13) Gong, C.; Li, L.; Li, Z.; Ji, H.; Stern, A.; Xia, Y.; Cao, T.; Bao, W.; Wang, C.; Wang, Y.; et al. Discovery of Intrinsic Ferromagnetism in Two-Dimensional van der Waals Crystals. *Nature* **2017**, *546* (7657), 265–269.
- (14) Shiomi, Y.; Takashima, R.; Saitoh, E. Experimental Evidence Consistent with a Magnon Nernst Effect in the Antiferromagnetic Insulator MnPS₃. *Phys. Rev. B* **2017**, *96* (13), 134425.
- (15) Lee, J. U.; Lee, S.; Ryoo, J. H.; Kang, S.; Kim, T. Y.; Kim, P.; Park, C. H.; Park, J. G.; Cheong, H. Ising-Type Magnetic Ordering in Atomically Thin FePS₃. *Nano Lett.* **2016**, *16* (12), 7433–7438.
- (16) Gibertini, M.; Koperski, M.; Morpurgo, A. F.; Novoselov, K. S. Magnetic 2D Materials and Heterostructures. *Nat. Nanotechnol.* **2019**, *14* (5), 408–419.
- (17) Ghazaryan, D.; Greenaway, M. T.; Wang, Z.; Guarochico-Moreira, V. H.; Vera-Marun, I. J.; Yin, J.; Liao, Y.; Morozov, S. V.; Kristanovski, O.; Lichtenstein, A. I.; et al. Magnon-Assisted Tunnelling in van der Waals Heterostructures Based on CrBr₃. *Nat. Electron.* **2018**, *1* (6), 344–349.
- (18) Shcherbakov, D.; Stepanov, P.; Weber, D.; Wang, Y.; Hu, J.; Zhu, Y.; Watanabe, K.;

- Taniguchi, T.; Mao, Z.; Windl, W.; et al. Raman Spectroscopy, Photocatalytic Degradation, and Stabilization of Atomically Thin Chromium Tri-Iodide. *Nano Lett.* **2018**, *18* (7), 4214–4219.
- (19) Frisenda, R.; Navarro-Moratalla, E.; Gant, P.; Pérez De Lara, D.; Jarillo-Herrero, P.; Gorbachev, R. V.; Castellanos-Gomez, A. Recent Progress in the Assembly of Nanodevices and van der Waals Heterostructures by Deterministic Placement of 2D Materials. *Chem. Soc. Rev.* **2017**, *47* (1), 53–68.
- (20) Hopkinson, D. G.; Zólyomi, V.; Rooney, A. P.; Clark, N.; Terry, D. J.; Hamer, M.; Lewis, D. J.; Allen, C. S.; Kirkland, A. I.; Andreev, Y.; et al. Formation and Healing of Defects in Atomically Thin GaSe and InSe. *ACS Nano* **2019**, *13* (5), 5112–5123.
- (21) Eichler, A.; Moser, J.; Chaste, J.; Zdrojek, M.; Wilson-Rae, I.; Bachtold, A. Nonlinear Damping in Mechanical Resonators Made from Carbon Nanotubes and Graphene. *Nat. Nanotechnol.* **2011**, *6* (6), 339–342.
- (22) Lee, J.; Wang, Z.; He, K.; Shan, J.; Feng, P. X. L. High Frequency MoS₂ Nanomechanical Resonators. *ACS Nano* **2013**, *7* (7), 6086–6091.
- (23) Will, M.; Hamer, M.; Müller, M.; Noury, A.; Weber, P.; Bachtold, A.; Gorbachev, R. V.; Stampfer, C.; Güttinger, J. High Quality Factor Graphene-Based Two-Dimensional Heterostructure Mechanical Resonator. *Nano Lett.* **2017**, *17* (10), 5950–5955.
- (24) Nair, R. R.; Blake, P.; Grigorenko, A. N.; Novoselov, K. S.; Booth, T. J.; Stauber, T.; Peres, N. M. R.; Geim, A. K. Fine Structure Constant Defines Visual Transparency of Graphene. *Science* **2008**, *320* (5881), 1308.
- (25) Meyer, J. C.; Girit, C. O.; Crommie, M. F.; Zettl, A. Hydrocarbon Lithography on Graphene Membranes. *Appl. Phys. Lett.* **2008**, *92* (12), 123110.

- (26) Suk, J. W.; Kitt, A.; Magnuson, C. W.; Hao, Y.; Ahmed, S.; An, J.; Swan, A. K.; Goldberg, B. B.; Ruoff, R. S. Transfer of CVD-Grown Monolayer Graphene onto Arbitrary Substrates. *ACS Nano* **2011**, *5* (9), 6916–6924.
- (27) Nagyte, V.; Kelly, D. J.; Felten, A.; Picardi, G.; Shin, Y.; Alieva, A.; Worsley, R. E.; Parvez, K.; Dehm, S.; Krupke, R.; et al. Raman Fingerprints of Graphene Produced by Anodic Electrochemical Exfoliation. *Nano Lett.* **2020**, *20* (5), 3411–3419.
- (28) Zan, R.; Ramasse, Q. M.; Jalil, R.; Georgiou, T.; Bangert, U.; Novoselov, K. S. Control of Radiation Damage in MoS₂ by Graphene Encapsulation. *ACS Nano* **2013**, *7* (11), 10167–10174.
- (29) Wagner, S.; Weisenstein, C.; Smith, A. D.; Östling, M.; Kataria, S.; Lemme, M. C. Graphene Transfer Methods for the Fabrication of Membrane-Based NEMS Devices. *Microelectron. Eng.* **2016**, *159*, 108–113.
- (30) Zheng, L.; Chen, Y.; Li, N.; Zhang, J.; Liu, N.; Liu, J.; Dang, W.; Deng, B.; Li, Y.; Gao, X.; et al. Robust Ultraclean Atomically Thin Membranes for Atomic-Resolution Electron Microscopy. *Nat. Commun.* **2020**, *11* (1), 1–8.
- (31) Lin, Y. C.; Lu, C. C.; Yeh, C. H.; Jin, C.; Suenaga, K.; Chiu, P. W. Graphene Annealing: How Clean Can It Be? *Nano Lett.* **2012**, *12* (1), 414–419.
- (32) Pettes, M. T.; Jo, I.; Yao, Z.; Shi, L. Influence of Polymeric Residue on the Thermal Conductivity of Suspended Bilayer Graphene. *Nano Lett.* **2011**, *11* (3), 1195–1200.
- (33) Dean, C. R.; Young, a F.; Meric, I.; Lee, C.; Wang, L.; Sorgenfrei, S.; Watanabe, K.; Taniguchi, T.; Kim, P.; Shepard, K. L.; et al. Boron Nitride Substrates for High-Quality Graphene Electronics. *Nat. Nanotechnol.* **2010**, *5* (10), 722–726.
- (34) Cao, Y.; Mishchenko, A.; Yu, G. L.; Khestanova, E.; Rooney, A. P.; Prestat, E.; Kretinin,

- A. V.; Blake, P.; Shalom, M. B.; Woods, C.; et al. Quality Heterostructures from Two-Dimensional Crystals Unstable in Air by Their Assembly in Inert Atmosphere. *Nano Lett.* **2015**, *15* (8), 4914–4921.
- (35) Andrade, E. N. D. C.; Martindale, J. G. The Structure and Physical Properties of Thin Films of Metal on Solid Surfaces. *Philos. Trans. R. Soc. A Math. Phys. Eng. Sci.* **1935**, *235* (747), 69–100.
- (36) 2D Semiconductors, <https://www.2dsemiconductors.com/full-area-coverage-few-layer-MoS2/>, (accessed June 2020).
- (37) Barthel, J.; Thust, A. On the Optical Stability of High-Resolution Transmission Electron Microscopes. *Ultramicroscopy* **2013**, *134*, 6–17.
- (38) Kelly, D. J.; Zhou, M.; Clark, N.; Hamer, M. J.; Lewis, E. A.; Rakowski, A. M.; Haigh, S. J.; Gorbachev, R. V. Nanometer Resolution Elemental Mapping in Graphene-Based TEM Liquid Cells. *Nano Lett.* **2018**, *18* (2), 1168–1174.
- (39) Algara-Siller, G.; Kurasch, S.; Sedighi, M.; Lehtinen, O.; Kaiser, U. The Pristine Atomic Structure of MoS₂ Monolayer Protected from Electron Radiation Damage by Graphene. *Appl. Phys. Lett.* **2013**, *103* (20), 203107.
- (40) Weston, A.; Zou, Y.; Enaldiev, V.; Summerfield, A.; Clark, N.; Z'olyomi, V.; Graham, A.; Yelgel, C.; Magorrian, S.; Zhou, M.; et al. Atomic Reconstruction in Twisted Bilayers of Transition Metal Dichalcogenides. *arXiv Prepr.* **2019**, 1911.12664.
- (41) Haigh, S. J.; Gholinia, A.; Jalil, R.; Romani, S.; Britnell, L.; Elias, D. C.; Novoselov, K. S.; Ponomarenko, L. A.; Geim, A. K.; Gorbachev, R. Cross-Sectional Imaging of Individual Layers and Buried Interfaces of Graphene-Based Heterostructures and Superlattices. *Nat. Mater.* **2012**, *11* (9), 764–767.

- (42) Clark, N.; Nguyen, L.; Hamer, M. J.; Schedin, F.; Lewis, E. A.; Prestat, E.; Garner, A.; Cao, Y.; Zhu, M.; Kashtiban, R. J.; et al. Scalable Patterning of Encapsulated Black Phosphorus. *Nano Lett.* **2018**, *18* (9), 5373–5381.
- (43) Bekaert, J.; Khestanova, E.; Hopkinson, D.; Birkbeck, J.; Clark, N.; Zhu, M.; Bandurin, D.; Gorbachev, R.; Fairclough, S.; Zou, Y.; et al. Enhanced Superconductivity in Few-Layer TaS₂ Due to Healing by Oxygenation. *Nano Lett.* **2020**, *20* (5), 3808–3818.
- (44) Dresselhaus, M. S.; Dresselhaus, G. Intercalation Compounds of Graphite. *Adv. Phys.* **1981**, *30* (2), 139–326.
- (45) Tsubokawa, I. On the Magnetic Properties of a CrBr₃ Single Crystal. *J. Phys. Soc. Japan* **1960**, *15* (9), 1664–1668.
- (46) Silbergliitt, R. Spin Waves in Ferromagnetic CrBr₃ Studied by Inelastic Neutron Scattering. *Phys. Rev. B* **1971**, *3* (1), 157.
- (47) Selska, K. N. videnskabers. *Forhandlinger-Det Kongelige Norske Videnskabers Selskab*, 5th ed.; Universitetsforlaget, 1932.
- (48) Chen, W.; Sun, Z.; Wang, Z.; Gu, L.; Xu, X.; Wu, S.; Gao, C. Direct Observation of van der Waals Stacking–Dependent Interlayer Magnetism. *Science* **2019**, *366* (6468), 983–987.
- (49) McGuire, M. A.; Dixit, H.; Cooper, V. R.; Sales, B. C. Coupling of Crystal Structure and Magnetism in the Layered, Ferromagnetic Insulator CrI₃. *Chem. Mater.* **2015**, *27* (2), 612–620.